

Circulation of the North Atlantic Ocean from altimetry and the Gravity Recovery and Climate Experiment geoid

Steven R. Jayne¹

Received 29 June 2005; revised 7 September 2005; accepted 8 November 2005; published 4 March 2006.

[1] We discuss the ocean circulation derived from the temporally averaged sea surface height, which is referenced to the recently released geoid from the Gravity Recovery and Climate Experiment (GRACE) mission (GRACE Gravity Model 02 (GGM02)). The creation of a precise, independent geoid allows for the calculation of the reference gravitational potential undulation surface, which is associated with the resting ocean surface height. This reference height is then removed from the temporally averaged sea surface height, leaving the dynamic ocean topography. At its most basic level the dynamic ocean topography can be related to the ocean's surface circulation through geostrophy. This has previously been impracticable because of large uncertainties in previous estimates of the Earth's geoid. Prior geoids included the temporally averaged sea surface from altimeters as a proxy for the geoid and therefore were unsuitable for calculations of the ocean's circulation. Geoid undulations are calculated from the GRACE geoid and compared to those from the NASA Goddard Space Flight Center and National Imagery and Mapping Agency Joint Earth Geopotential Model (EGM96) geoid. Error estimates are made to assess the accuracy of the new geoid. The deep ocean pressure field is also estimated by combining the calculated dynamic ocean topography with hydrography. Finally, the derived circulation is compared to independent observations of the circulation from sea surface drifters and subsurface floats. It is shown that the GGM02 geoid is significantly more accurate for use in estimating the ocean's circulation.

Citation: Jayne, S. R. (2006), Circulation of the North Atlantic Ocean from altimetry and the Gravity Recovery and Climate Experiment geoid, *J. Geophys. Res.*, *111*, C03005, doi:10.1029/2005JC003128.

1. Introduction

[2] The sea surface height observed by satellite altimeters contains signals from many different phenomena. There are contributions from changes in the Earth's gravity field (the geoid), the tides, the atmospheric pressure (the inverted barometer effect), and the ocean's circulation [Chelton, 1988; Tapley and Kim, 2001]. What is commonly referred to as the sea surface height in numerical ocean general circulation models is really just the last of these, that is the part of the sea surface height that arises from the ocean's circulation and is referred to as the dynamic ocean topography. In the simplest case, the gradient of the dynamic ocean topography can be related to the surface velocity field through geostrophy. One of the great promises of satellite altimetry was that it would reveal the geostrophic surface ocean circulation by observing the dynamic ocean topography. Observation of the dynamic ocean topography from satellite altimeters requires a good estimate of the Earth's geoid to separate out the changes in the sea surface height because of the varying height of the constant gravitational

potential surface from those height changes arising from the ocean's circulation. To date, however, the utilization of the time-averaged part of the dynamic ocean topography has suffered from inadequate estimates of the Earth's geoid. The spatial changes in the geoid height are approximately 100 times larger than those associated with the dynamic ocean topography. Therefore even small errors in the knowledge of the geoid have prevented the use of the time-averaged sea surface height for accurately determining the time-mean surface circulation from altimetry. Now, with the launch of a dedicated gravity satellite mission to determine the geoid, the Gravity Recovery and Climate Experiment (GRACE) has now provided an independent estimate of the geoid [Tapley *et al.*, 2004].

[3] Hydrographic observations of the ocean's density field have long been used to infer the ocean's velocity field through the thermal wind equations. However, the thermal wind relation can only provide the vertical shear of the horizontal velocity, so that when it is integrated in depth to provide the velocity field, an integration constant is missing. This integration constant is the velocity at the starting point of the vertical integration, often referred to as the reference level. This missing piece of the velocity field arises because there is an external part of the pressure field from the presence of gradients in the dynamic ocean topography, which until recently have not been observable. The velocity

¹Woods Hole Oceanographic Institution, Woods Hole, Massachusetts, USA.

at the reference level needs to be provided from another data source, which is generally lacking. There is a long history of inferring the velocity at the reference level through ad hoc assumptions, such as a level of no motion, or more rigorously through inverse methods (i.e., the β -spiral method used by *Olbers et al.* [1985]). Direct observation of the dynamic ocean topography provides the necessary reference velocity such that when combined hydrographic observations, the full geostrophic velocity field can be calculated.

[4] *Wunsch and Gaposchkin* [1980] reviewed the basic problem of combining observations of sea surface height, the geoid, and hydrography together to estimate the ocean's pressure field without an arbitrary level of no motion, and hence from that the ocean's full (baroclinic plus barotropic) geostrophic circulation. However, lacking an independent geoid, attempts in the past to utilize their methodology to estimate the temporal mean sea surface height have met with mixed success. *Zlotnicki* [1984] made an early comparison of sea surface height from SeaSAT and the known geoid over the North Atlantic Ocean. At the time the geoid was poorly known and errors of over a 2.5 m were seen in some areas. Since the expected magnitude of the sea surface height signal from the ocean's circulation is of order 1 m, the estimate was largely useless as even a qualitative description of the temporal mean circulation in the North Atlantic.

[5] Improvements in estimates of the geoid came with additional satellite altimetry data, satellite tracking data, and surface gravity observations. These estimates of the geoid culminated with the NASA Goddard Space Flight Center and National Imagery and Mapping Agency Joint Earth Geopotential Model (EGM96) geoid estimation by *Lemoine et al.* [1998]. Using the EGM96 to estimate the departure of the sea surface, as observed by satellite altimetry, from the level of constant geopotential, it was possible to see the large-scale circulation as envisioned by *Wunsch and Gaposchkin* [1980]. However, the EGM96 geoid (and others like it such as, OSU91 by *Rapp et al.* [1991], JGM3 by *Tapley et al.* [1996] and GRIM5 by *Gruber et al.* [2000]), are not independent estimates of the geoid since they incorporate large amounts of satellite altimetry data over the oceans as geoid observations. For the specific purpose of estimating the geoid, this is not a bad methodology since the variations in the geoid are about 100 times larger than the signals arising from the ocean circulation. However, for the purpose of estimating the ocean circulation this is problematic because some of the ocean's dynamic topography gets folded into the geoid, and then gets canceled out when the difference is taken between the altimeter-observed temporal mean sea surface and the geoid.

[6] Despite their inadequacies, the extant geoids are useful for observing the largest features of the general circulation. *Stammer and Wunsch* [1994] made a preliminary assessment of the TOPEX/Poseidon altimeter data and found on the largest scales a circulation consistent with observational estimates and a numerical model. Improvements to the geoid could be made by combining the sea surface height, the geoid, and a numerical model, using an adjoint to minimize the differences between the observations and model [*Wunsch and Stammer*, 1998, 2003]. However, for the problem of estimating the global transports of heat and mass by the ocean, the geoids were not

sufficiently accurate [*Ganachaud et al.*, 1997; *Schröter et al.*, 2002]. Most of these prior studies determined that ultimately a dedicated gravity mission that would independently measure the geoid was required in order to adequately utilize the temporal mean sea surface height to infer the ocean circulation.

[7] The Gravity Recovery and Climate Experiment (GRACE) is a joint U.S. and German satellite mission by NASA and the Zentrum für Luft-und Raumfahrt (for a description of the mission see *Davis et al.* [1999], *Dunn et al.* [2003], *Tapley et al.* [2003a], and *Reigber et al.* [2005]). It was launched on 17 March 2002 and it is expected to have a nominal lifetime of 5 years. The mission consists of two satellites, in identical orbits with initial altitudes near 500 km, with one trailing the other by about 200 km. The satellites range between each other using microwave tracking system, and the geocentric position of each spacecraft is monitored using onboard GPS receivers. Onboard accelerometers measure the nongravitational accelerations (i.e., atmospheric drag) so that their effects can be removed from the satellite-to-satellite distance measurements. The residual gravitational accelerations are used to map the Earth's gravity field orders of magnitude more accurately, and to considerably higher spatial resolution, than by any previous geoid estimate [*Tapley et al.*, 2003a].

[8] *Tapley et al.* [2003b] describe an initial look at the large-scale ocean circulation derived from the first GRACE geoid (GGM01). In that paper, they attempted to validate the estimated dynamic ocean topography by comparing it against the steric ocean height calculated from a hydrographic climatology [*Stephens et al.*, 2002]. They compared the time-averaged dynamic ocean topography estimated using the GRACE Gravity Model 02 (GGM02) geoid to reference the altimeter observations against that estimated using the older EGM96 geoid [*Lemoine et al.*, 1998]. However, beyond a qualitative comparison of the surface geostrophic circulation estimated from them, they did not attempt to assess the accuracy of the geoids on different length scales. Additionally, the comparison of the pressure and velocity fields estimated from the observed dynamic topography to those estimated from dynamic height from hydrography neglects the contribution of the barotropic component of the pressure and velocity fields that is present in the dynamic topography but missing in the dynamic height.

[9] This paper is an attempt to quantify the accuracy of the geoid over a range of wavelengths, and to present a method of assessing the improvement in the geoid using an independent data set. We compute the dynamic ocean topography related to the temporal mean ocean circulation from the combination of the sea surface height observed by satellite altimetry and the geoid observed by GRACE. We compute the pressure field for two depths by combining the estimated sea surface pressure field with hydrographic observations. We then estimate the geostrophic velocity fields from the surface and deep pressure fields, and these are compared to observed velocities from floats and drifters. The temporal mean geoid estimated by the GRACE mission is continually evolving as new observations are obtained and the geoid estimation techniques are being improved. Therefore, for the purposes of this paper we do not compare the relative merits of the different geoids generated by the

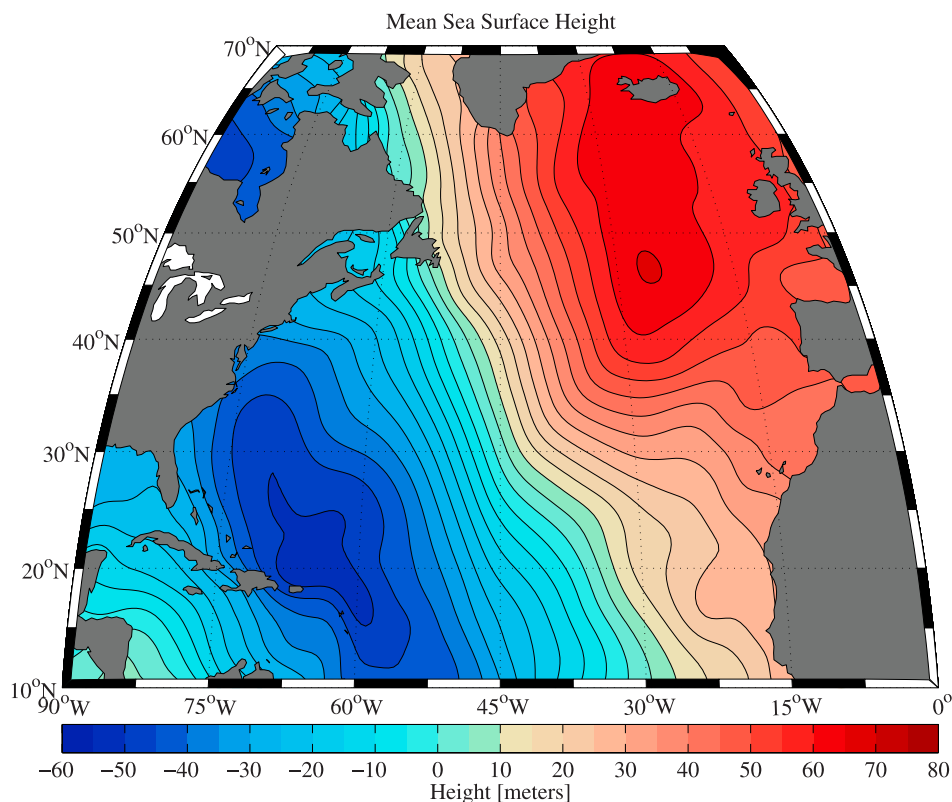


Figure 1. Mean sea surface height, smoothed from the CLS01 sea surface height for $N = 60$, for a resolution of approximately 333 km.

GRACE program, of which there are now several iterations, but rather, we attempt to show the large increment in accuracy of the geoid that GRACE mission has produced, review it uses for physical oceanographic purposes, and show that the GGM02 geoid is now sufficiently accurate to permit the combination of in situ observations.

2. Data Sources

[10] To perform this analysis, a variety of data sources were required. They were (1) the temporally averaged sea surface height, the height of the ocean surface observed by satellite altimeters and averaged in time; (2) the geoid, as estimated by the GRACE mission, as well as a previous estimate (EGM96) made before the gravity satellite mission; (3) hydrographic data from a historical climatology of temperature and salinity observations; (4) surface drifters that track the movement of the near surface ocean circulation; and (5) subsurface floats that track the movement of the deep ocean circulation. The particulars and details of these data sets are discussed below.

2.1. Time-Averaged Sea Surface Height

[11] The CLS01 time-averaged sea surface height was used for this study [Hernandez and Schaeffer, 2000, also The CLS01 mean sea surface: A validation with the GSFC00.1 surface, 2001, available at <http://www.cls.fr/mss/>]. The mean sea surface has been computed using data from a 7-year TOPEX/Poseidon time-averaged profile, a 5-year ERS-1/2 time-averaged profile, a 2-year GEOSAT time-averaged profile, and the two 168-day nonrepeat

cycles of the ERS-1 geodetic phase. The time-averaged sea surface height is defined on a $2'$ ($1/30^\circ$) grid, between 80°S and 82°N . Over the ocean, the data come from the satellite altimeters, and over land, the surface is filled in with values from the EGM96 geoid. In coastal areas (between ocean and land) a smooth extrapolation of the ocean values (which includes both the mean dynamic topography and the geoid) toward the EGM96 geoid that was used. An important aspect of this data product is that it comes with an estimation of its error field, since this allows us to estimate the error in the dynamic ocean topography after referencing it to the geoid. The sea surface height is smoothed in space with a filter described in section 3, and is shown in Figure 1.

[12] The 7-year mean TOPEX profile is the average from 1993–1999, whereas the other altimeter data cover different time epochs, they are all adjusted to the TOPEX mean profile, and therefore the resulting mean sea surface height can be said to represent the time average from 1993 to 1999, in as much as the interannual changes in the sea surface height occur over large spatial scales that are observable by TOPEX/Poseidon. Other time-averaged sea surface height analyses exist, such as the GSFC98 [Wang, 2000] and KMS04 [Andersen et al., 2004], and these were examined as well, however, it was found that the CLS01 product gave the most consistent circulation maps, and we will use it throughout.

2.2. The Geoid

[13] The second GRACE geoid released by the Center for Space Research at the University of Texas (GGM02C) (for a description see Tapley et al. [2005]) was used to

synthesize the geoid undulation on a geodetic 2' grid, consistent with the mean sea surface height. The geoid undulation was computed using the geoid synthesis program by *Smith* [1998] for a reference ellipsoid consistent with the CLS01 mean sea surface. For reference, the CLS01 mean sea surface product uses the TOPEX/Poseidon Earth ellipsoid, with an Earth radius of 6378136.3 m, a flattening of 1/298.257, and a gravitational mass of $398600.4415 \text{ km}^3 \text{ s}^{-2}$, for a gravity potential surface of $62636858.702 \text{ m}^2 \text{ s}^{-2}$ so as to be consistent with the geodetic reference frame used by the Pathfinder altimeter products, and is defined in International Terrestrial Reference Frame [McCarthy, 1996]. The map of geoid undulation was smoothed in a manner identical to the sea surface height. Since the changes in the height of the geopotential surface are approximately 2 orders of magnitude larger than changes in the dynamic ocean topography, the smoothed geopotential looks nearly identical to the sea surface height at these scales.

[14] The geoid is synthesized from a set of spherical harmonic coefficients which define the mass field of the Earth and are the end product of a large least squares combination of the satellite gravity observations made by GRACE. The field we require is the spatially varying height of a constant gravitational potential surface relative to the reference ellipsoid that most closely matches the mean sea surface height. This is called the geoid undulation. The geoid undulation is solved for iteratively from the geoid's spherical harmonic coefficients as solution to the Bruns equation. Care must be taken when synthesizing the geoid undulation from the spherical harmonic coefficients for a given geoid to do so in geodetic latitude [Smith, 1998]. Further details of the synthesis program to calculate the geoid undulation are given by *Smith* [1998].

[15] Another subtle point that needs to be addressed when synthesizing the geoid undulation for use in physical oceanography applications is the treatment of the mean tide. The geopotential field of the Earth can be realized using three different treatments of the mean tide, and because the potential field can be defined under these different permanent tide systems, it is necessary that the geoid undulation and the sea surface height are referenced to the same system. The mean tide results from the presence of the sun and moon which induces a time-mean tidal deformation of the oceans and the solid earth (about 20 cm from equator to pole). The mean tide is the permanent perturbation of the Earth's gravitational field by the presence of external bodies (mainly the Moon and the Sun). The "mean tide" potential corresponds to the gravitational potential that exists from the combined effects of the Earth, the Moon and the Sun. The geoid undulation computed relative to the chosen potential surface for this would correspond to the temporal mean ocean surface in the absence of any nongravitational disturbances (currents, winds, heating, evaporation, precipitation, etc.) It corresponds most directly to what a satellite altimeter measures when observing the sea surface height from space.

[16] The two other treatments are termed the "zero-tide" and "tide free." In the zero-tide convention is the potential field field that would occur if the direct contributions of the Moon and Sun to the gravity field at the Earth's surface where removed. The tide-free treatment goes on further to remove the *indirect* perturbations to the gravity field arising

from the displacement of the mass of the Earth (both the solid and its fluid shell) deforming under the external gravity perturbations that cause the mean tide. This system requires an assumption for the load Love number (usually taken as $k = 0.3$) (for a more extensive discussion see *Smith* [1998] and *Lemoine et al.* [1998]).

[17] The time-averaged sea surface heights and geoids used in this work use the following different treatments of the time-mean tide:

[18] 1. In the mean tide system, no adjustment is made to the mean tide. The height of the undulation in this system is as would be directly observed by an altimeter. The CLS01 mean sea surface height product use this convention.

[19] 2. In the zero-tide system the ocean mean tide is removed (direct effect), but the solid earth deformation resulting from the ocean mean tide is left in (indirect effect). The GRACE geoids from University of Texas (CSR) and NASA JPL use this convention.

[20] 3. In the tide-free (or nontidal) system both the direct and the indirect effects of the time-mean tide are removed. The EGM96 geoid uses this convention, as does the GRACE geoid computed by GeoForschungsZentrum Potsdam (GFZ).

[21] For this work, the geoid undulation was computed in the zero tide convention, and then transformed to the mean tide convention by the adding on the mean tide contribution to the undulation height [Lemoine et al., 1998]:

$$G_{\text{mean}} = G_{\text{zero}} + 9.9 - 29.6 \cos^2(\theta) \quad [\text{cm}], \quad (1)$$

where θ is the latitude.

2.3. Hydrography

[22] The dynamic height contribution to the pressure field is the part that arises from horizontal changes in temperature and salinity which have a combined effect on density. The dynamic height is a measure of the anomaly in the pressure field due to these density changes between two reference depths. A quality-controlled collection of hydrographic data from the North Atlantic was used to estimate the subsurface pressure field (Hydrobase Climatology of *Lozier et al.* [1995]). The temperature and salinity climatology consists of 97,160 profiles to 700 m, and 31,404 profiles to 2000 m depth. The temperature and salinity fields were used to calculate the dynamic height between the surface and 700 m, and the surface and 2000 m. These values were then bin-averaged to a nominal 1/4° grid and then linearly interpolated on to a regular 1/4° grid. The gridded values were then smoothed in space using the same filter as was used to smooth the sea surface height and the geoid undulation.

2.4. Surface Drifters

[23] Surface drifter displacements from the Surface Velocity Program data set [Pazan and Niiler, 2004], spanning the time period from 1992–2002, were used to estimate a time-averaged surface circulation. The drifter displacements were first corrected for the drift associated with the wind-driven Ekman velocity following the empirically derived fit of *Ralph and Niiler* [1999]. After removing the Ekman velocity, it is assumed that the remaining velocity is that of the large-scale geostrophic ocean circulation. The 1,881,959 drifter displacements were then averaged on to a

nominal $1^\circ \times 1^\circ$ grid, with the averaged velocity locations placed on the weighted centroids of the all the data contributing to any given bin, to give an estimate of the time-averaged velocity at that point.

2.5. Subsurface Floats

[24] Float displacements from a variety of subsurface float types (Argo, ALACE, BOBBER, P-ALACE, RAFOS, and SOFAR) from numerous deployments were used to estimate the time-averaged velocity fields at 700 and 2000 m. The methodology of *Lavender et al.* [2005] was followed to make an estimate of the velocity field at 700 m. The 281,813 float displacements between 200 to 1600 m, with an average depth of 747 m, were adjusted for the time-averaged vertical shear between their drift depth and 700 m, calculated from the Hydrobase climatology [*Lozier et al.*, 1995] assuming geostrophy. Following the same procedure as the surface drifters, the adjusted float displacements were then averaged on to a nominal $1^\circ \times 1^\circ$ grid, with the averaged velocity locations placed on the weighted position of the all the data contributing to any given bin, to give an estimate of the time-mean velocity at that centroid. For the estimated float velocity field at 2000 m, 33,646 float displacements between 1600 to 2600 m, with an average depth of 1970 m, were adjusted by the the time-averaged vertical shear to 2000 m and averaged in to spatial bins.

3. Smoothing Method

[25] The error in the geoid estimates produced by the GRACE mission increases rapidly (approximately exponentially) with decreasing wavelength. This arises from the attenuation of the gravity signal with increasing altitude above the surface of the Earth. The attenuation is stronger for the shorter features of the geoid, such that for GRACE at orbital height of 500 km, features shorter than a few hundred kilometers are not well observed by GRACE. What this practically means is that in synthesizing the geoid undulation from the spherical harmonic coefficients the summation must be cutoff at some wavelength (or equivalently some length scale) to suppress the noise at the high wave numbers (or short length scales). However this needs to be done smoothly, or ringing from the Gibbs phenomenon will result.

[26] The time-averaged sea surface is only defined over the ocean and is undefined over land. This presents a problem when applying spatial filters to both the geoid and sea surface height. While the geoid is naturally represented in harmonic space, it could be smoothed easily in the spectral domain. The sea surface height and hydrographic data are only naturally represented in physical space, and therefore are most readily smoothed in physical space. *Tapley et al.* [2003b] chose to convert the mean sea surface height into spherical harmonics to be consistent with the geoid, but smoothed the hydrography in physical space with a Gaussian smoother. Converting the mean sea surface height into spherical harmonics requires filling in the land values with a proxy for the geoid undulation for which *Tapley et al.* [2003b] chose EGM96. However, this introduces additional errors in the mean sea surface height. Therefore, while much more computationally time-consuming, we choose to filter

the geoid undulation and sea surface height in the spatial domain.

[27] Truncating the summation in harmonic space is equivalent to smoothing in physical space. A Gaussian smoother is often used [*Jekeli*, 1980] since its spectral characteristics are well known, and it is Gaussian in both wave number and physical spaces. However, in this application, we have chosen to use a Hamming window smoother, which is given by the equation

$$F(\gamma) = \begin{cases} 0.54 + 0.46 \cos(N\gamma) & \gamma \leq \pi/N \\ 0 & \gamma > \pi/N \end{cases}, \quad (2)$$

where γ is the angle between two points (θ_1, ϕ_1) and (θ_2, ϕ_2) on the surface of the Earth, given by $\cos \gamma = \sin \theta_1 \sin \theta_2 + \cos \theta_1 \cos \theta_2 \cos(\phi_1 - \phi_2)$. This particular filter was selected for a few reasons. The Hamming window has a well defined cutoff in wave number number space (and a corresponding wavelength) while the Gaussian filter trails off indefinitely. Also the Hamming window minimizes the sidelobes in the wave number domain [*Priestley*, 1981]. Finally, the Hamming window has a finite spatial domain where a Gaussian window includes all the points on the sphere. The latter point will be important for our application. The value of N defines the cutoff wave number for the filter. At a wave number of $2N$ the power spectrum of the filter tails off to zero. It defines an approximate resolution (Δ) of the smoothed field, given by

$$\Delta = \frac{2\pi \cdot 6371}{2N} \text{ km}. \quad (3)$$

[28] Where the spatial filter encompasses land points a subjective decision must be made. The mean sea surface height products fill the land values with the value of the geoid undulation from whichever geoid they are referenced to, hence this introduces spurious values into the smoothed sea surface height in any point that includes land values. If the same geoid were used to reference the mean sea surface height as was being removed, this would result in zeros being averaged into the smoothed dynamic ocean topography, however, because the currently available mean sea surface products use older, less accurate geoids, this introduces additional geoid errors in the to smoothed dynamic ocean topography near land. With Gaussian filters this is more problematic since, strictly speaking, every smoothed value over the ocean would include land points as well. The Hamming window lessens this problem to some extent, but any point within one smoothing radius of land will still be contaminated.

[29] The other choice is to not include in the filter those points over land and near the coasts. While this disrupts the spectral characteristics of the filter, it is the method we have chosen to avoid biasing the dynamic ocean topography near land to zero. In the smoothing calculations, we drop from the filtered value all sea surface height points flagged as over land, as well as those points that have an extrapolated value over the coasts. As a result, these smoothed values will have a

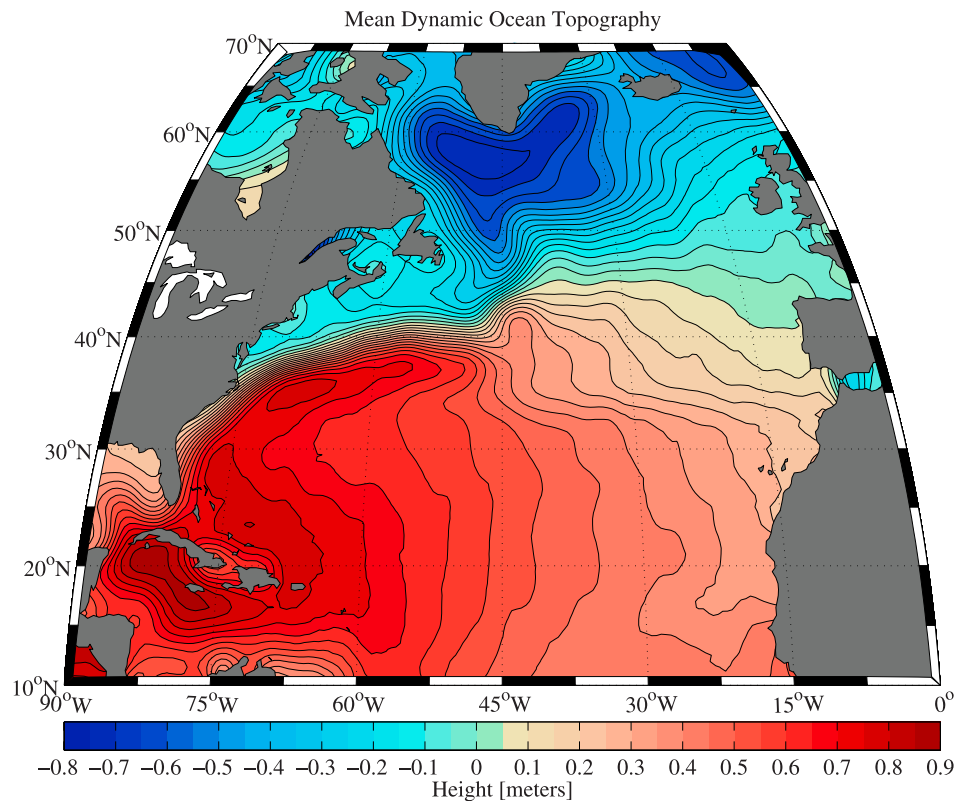


Figure 2. Dynamic ocean topography, showing difference of smoothed fields from the CLS01 sea surface height and GRACE geoid. Pressure is in units of equivalent sea surface height. To retrieve pressure, multiply by gravity and density ($9.8 \text{ m s}^{-2} \times 1025 \text{ kg m}^{-3}$).

higher error associated with them, but will be free of contamination from land points.

4. Maps

[30] The dynamic ocean topography is the difference between the sea surface and the geoid undulation, and the smoothed field for $N = 60$ ($\Delta = 333 \text{ km}$) is shown in Figure 2 as the dynamic ocean topography. The dynamic ocean topography is directly related to the surface pressure field and can be obtained by multiplying it by gravity (9.806 m s^{-2}) and the density of sea water (1025 kg m^{-3}). The surface pressure field shows a circulation field consistent with our general understanding of the ocean's temporally averaged circulation based on historical observations. A broad, strong Gulf Stream moves along the East Coast of North America and separates from the coast at Cape Hatteras. South of the stream, there is the signature of a strong southern recirculation gyre, while there is little sign of a northern recirculation gyre in the dynamic ocean topography. At the Northwest Corner, the North Atlantic Current spreads, with part moving northeastward toward Europe, and part going into the broad southward flow of the Sverdrup circulation. There is some suggestion of the Mann eddy [Mann, 1967], though there is not a closed pressure contour at the surface. South of Greenland, there is the strong cyclonic circulation of the subpolar gyre.

[31] There are also some unrealistic features in the pressure field such as the strong low around the southern

end of Cuba and Hispaniola, and another low just north of South America. Apparently, these errors are in the mean sea surface height product and arise from the blending of the EGM96 geoid with the observed sea surface height near land. Additionally, the Gulf Stream appears to connect with the circulation in the Gulf of Mexico by crossing Florida. This latter feature results from the relatively heavy smoothing that still must be applied to the geoid to suppress noise at the shorter spatial scales.

[32] A comparison can be made to the global map of absolute sea level estimated from drogued surface drifters by Niiler *et al.* [2003]. Their map used the same drifter data set described in section 2.4, which they used to estimate an absolute sea level map for the global ocean. Their values for the sea level differences across two transects of the North Atlantic Ocean basin are reported in Table 1. As a point of comparison, they also computed an estimate of the steric height between the surface and 3000 m from the World Ocean Atlas (WOA01) hydrographic climatology [Stephens *et al.*, 2002]. The first cross basin pressure difference is the east-west pressure gradient across the gyre from the high near the Gulf Stream in the west to the eastern edge of the basin along 30°N . In the historical analysis by Reid [1994], the pressure difference is 55 cm, and the difference here is 51 cm. Niiler *et al.* [2003] find a difference of only 35 cm, which they attribute to the presence of a strong narrow Azores Current not present in the Reid analysis or the hydrography, and given the smoothing scales used here would not be present in our analysis either. The EGM96

Table 1. Dynamic Ocean Topography Difference Across the North Atlantic Basin Along Two Transects^a

Cross section	Reid	WOA01	Niiler et al.	GRACE	EGM96
30°N, 75°W–30°N, 15°W	55	50	35	51	32
30°N, 75°W–60°N, 45°W	133	137	121	132	109

^aHeight differences are in centimeters. Values are reported from Reid [1994], dynamic height from 0 to 3000 m is from World Ocean Atlas (WOA01) [Stephens et al., 2002], and from Niiler et al. [2003], and the dynamic ocean topography is computed using the GRACE geoid and the EGM96 geoid.

geoid gives a weaker pressure difference of 32 cm. Similar trends are seen in the pressure difference between the subtropical high and subpolar low, with the Reid analysis, the hydrography and the dynamic ocean topography with all having pressure differences in the range of 132–137 cm. The Niiler analysis is again lower at 121 cm, and the dynamic ocean topography evaluated using the EGM96 geoid is only 109 cm. It appears that the dynamic ocean topography evaluated with the GRACE geoid is consistent with historical analyses and hydrography.

[33] Because of the smoothing applied to the fields, the estimated Gulf Stream is too broad and its velocities are too

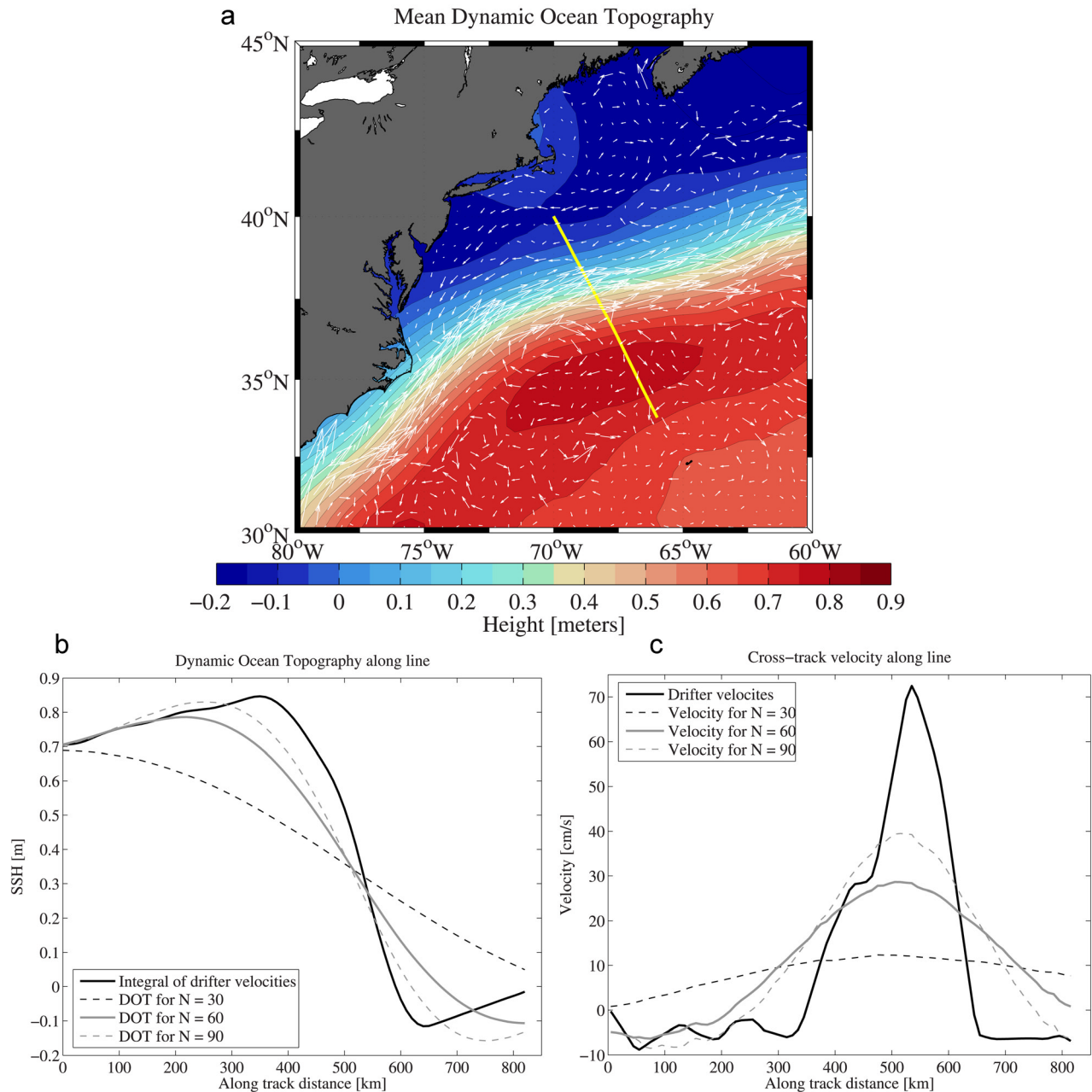


Figure 3. (a) Estimated dynamic ocean topography elevation from drifter observations (assuming geostrophy) and estimates from the observed sea surface height and geoid for various smoothing scales. (b) Observed cross-track velocities from drifter observations and (c) observed dynamic ocean topography for various smoothing scales.

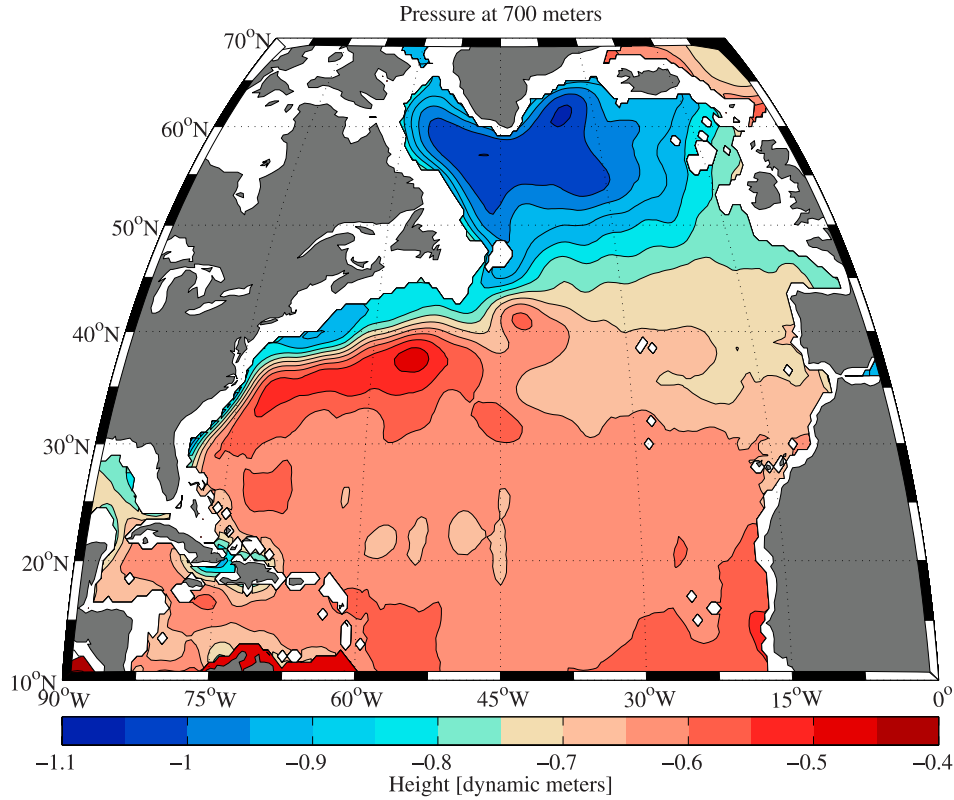


Figure 4. Pressure at 700 m, showing difference of smoothed fields from the CLS01 sea surface height and GRACE geoid combined with dynamic height from 0 to 700 m. Pressure is in units of equivalent sea surface height. To retrieve pressure, multiply by gravity and density ($9.8 \text{ m s}^{-2} \times 1025 \text{ kg m}^{-3}$).

low. In a synoptic section, the Gulf Stream is a narrow jet, on the order of 50 km in width. Over time, it meanders strongly, having the effect of smoothing and broadening it in the temporal average. However, even in the temporal mean the Gulf Stream should be narrower, as is shown in Figure 3b. Here we take the surface drifter observations (which have been corrected for Ekman drift [Pazan and Niiler, 2004]) and interpolated them to a TOPEX ground track that goes approximately between Bermuda and Cape Cod (see Figure 3a). Taking the component of the drifter velocities normal to the line, and assuming geostrophy, we can calculate the expected dynamic ocean topography along the line according to

$$\eta = - \int \frac{fu}{g} dl + \eta_0, \quad (4)$$

where f is the Coriolis parameter, u is the velocity component normal to the line we are integrating along, g is gravity, and η_0 is an unknown integration constant. For the purposes of comparison to the dynamic ocean topography, η_0 is set to the value of η from the altimeter at the southern end of the line for the smoothing case of $N = 60$. In Figure 3c, we do the opposite and take the along-track derivative of the dynamic topography for the various smoothing scales, and assuming geostrophy, calculate the cross-track velocity according to

$$u = - \frac{g}{f} \frac{\partial \eta}{\partial l}, \quad (5)$$

and compare this to the drifter velocity observations. It is apparent that the temporal mean Gulf Stream across this line as shown by the drifters is a narrower and stronger current than can be estimated from the dynamic topography estimated from the combination of the altimeter and geoid. As less smoothing is used in the spatial filter, the estimated current becomes stronger and narrower. However, the overall transport of the current, which is the difference between the maximum and minimum of the dynamic topography across the jet, is robust for all but the strongest smoothing ($N = 30$). Here we see a fundamental trade-off that must be made when calculating the dynamic topography, that is choosing between adequate resolution of the surface pressure gradients (and hence the estimated geostrophic current speeds) versus the need to smooth adequately to suppress noise in the short length scales of the geoid. The required amount of smoothing will then be determined by a given application, the robustness of the signal being sought, and noise levels.

[34] This approach is similar to Kelly *et al.* [1991] who examined the geoid and the mean sea surface along a GEOSAT ground track that also ran between Bermuda and Cape Cod. They utilized a shipboard ADCP to measure a synoptic section of the Gulf Stream's near surface circulation. Estimating the dynamic ocean topography from their velocity field, they found an approximately 1-m net height difference across the Gulf Stream in agreement with our estimate here, though their velocities were larger in magnitude than ours because of their use of a synoptic section versus the temporally averaged drifter observations used here.

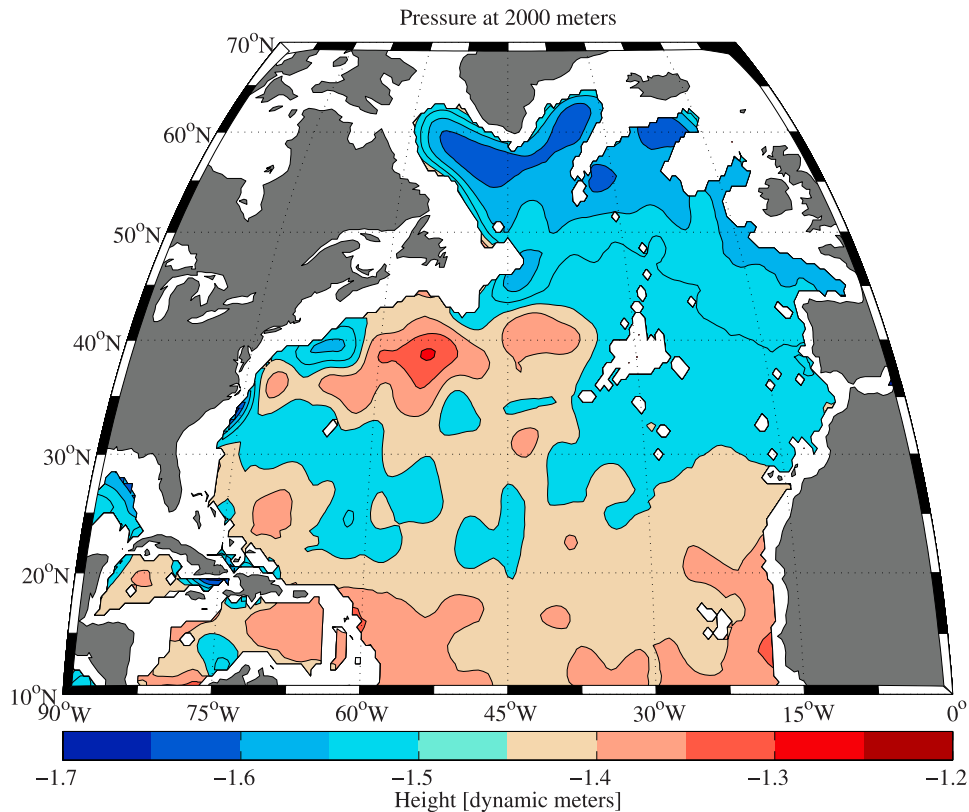


Figure 5. Pressure at 2000 m, showing difference of smoothed fields from the CLS01 sea surface height and GRACE geoid combined with dynamic height from 0 to 2000 m. Pressure is in units of equivalent sea surface height. To retrieve pressure, multiply by gravity and density ($9.8 \text{ m s}^{-2} \times 1025 \text{ kg m}^{-3}$).

[35] Moving deeper in the water column, we combine the dynamic ocean topography with the dynamic height from hydrography to obtain the pressure fields at 700 and 2000 m. In the estimated pressure at 700 m (Figure 4), we see the signature of the Gulf Stream remains (although somewhat weaker, with a cross-stream pressure gradient of 34 cm at this level compared to the surface pressure gradient of 87 cm). The southern recirculation gyre stands out with a strong pressure signal, and there is a sign of the northern recirculation gyre. The Mann eddy now is revealed as a closed pressure contour at this depth. In the subpolar gyre in the northern part of the basin, we can compare the derived circulation with that reported by *Lavender et al.* [2005]. Using an objective mapping of float observations, they found a circulation of approximately the same dynamic pressure difference between the deepest part of the subpolar low and the northern edge of the North Atlantic Current. However, their circulation is much tighter, and their current speeds are stronger, as expected by our need to spatially smooth our pressure field. In the southern portions of the basin, there is very little apparent pressure gradient across the basin. Again, the circulation is noisy in the area around Hispaniola and in the Caribbean. At 2000 m (Figure 5), the pressure field becomes noisy, there are still suggestions of the recirculation gyres that flank the Gulf Stream, and the subpolar low still has a strong circulation at this depth. However, in the interior of the basin the field is probably mostly noise.

[36] Finally, we can compare the circulation derived from the GRACE geoid to that derived from the EGM96 geoid. In Figure 6 is shown the dynamic ocean topography using EGM96 which can be compared to Figure 2. It is seen that while there are some qualitative similarities, the flow is far too broad and diffuse. In Figure 7 the pressure at 700 m calculated using EGM96 and hydrography, which can be directly compared to Figure 4. At 700 m there are not even many qualitative similarities, as the flow in the region of the Gulf Stream is in the wrong direction.

5. Error Analysis

[37] In as much as it is useful to produce maps of the pressure field and its related circulation, it is equally important to quantify the error in the estimated fields. This is particularly important now that data assimilation efforts are becoming common, since it is envisioned that the surface pressure fields will be assimilated into numerical models or otherwise used in statistical estimations with other data types. These techniques require estimates of the error covariance associated with the estimates.

[38] A key concept to understand when assessing the errors in the geoid and the resulting dynamic ocean topography is the idea that the total error in the geoid is composed of errors of omission and errors of commission. The errors of commission are the errors that are included in the calculated field arising from the errors in the estimated spherical harmonics of the geoid. The errors of omission are

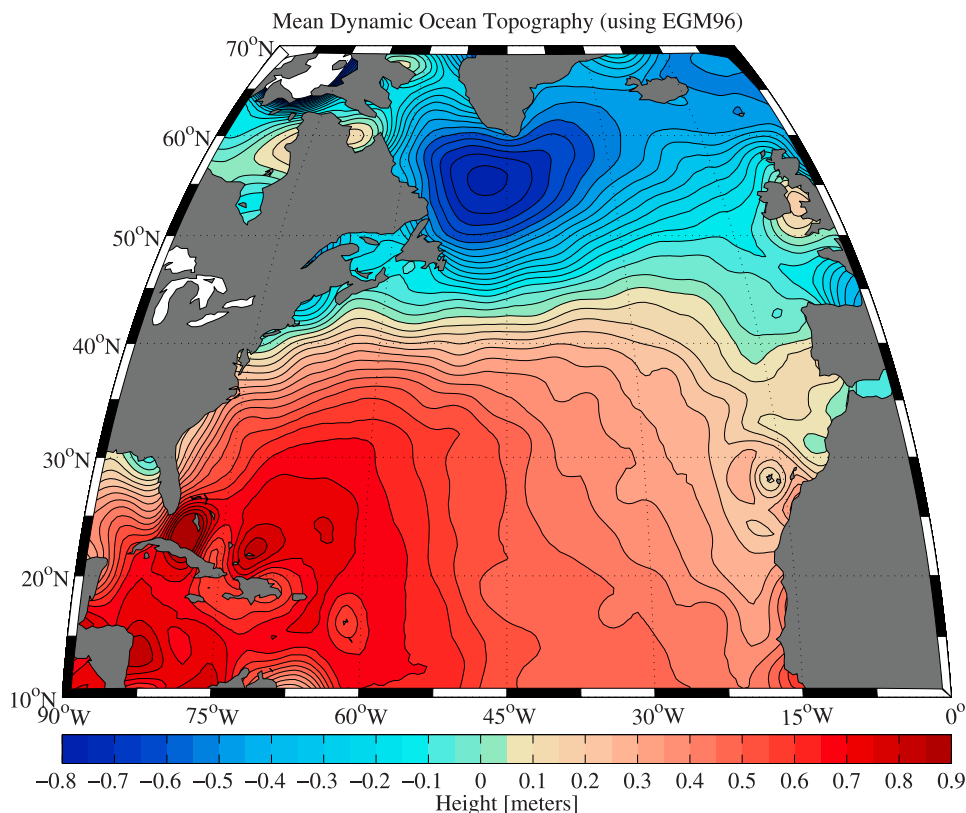


Figure 6. Dynamic ocean topography, showing difference of smoothed fields from the CLS01 sea surface height and EGM96 geoid. Pressure is in units of equivalent sea surface height. To retrieve pressure, multiply by gravity and density ($9.8 \text{ m s}^{-2} \times 1025 \text{ kg m}^{-3}$).

the errors in the estimated fields that result from truncating the summation of the spherical harmonics at some cutoff wave number (spatially smoothing the field). Thus the total error in the calculated field results from two parts: (1) errors in the part of the spectrum that is included in the estimate (errors of commission) and (2) errors resulting from truncating the spectrum at some wave number (errors of omission). The reason for truncating the spectrum is that the committed error in GRACE's estimates of the higher wave numbers of the geoid increase exponentially. Hence by truncating the summation of the spherical harmonics at some wave number, we reduce the total committed error at the cost of creating an error of omission by not including the shorter wavelengths. For our purposes here the committed errors can be estimated by comparing the different geoids at various wavelengths to each other, and thus gaining some insight into the uncertainty of the estimated geoid undulation. The omitted errors are harder to quantify since to do so requires an estimation of the errors that result from excluding the higher wavelengths of the geoid. Here we do so by comparing the geostrophic velocity field calculated from the dynamic ocean topography and hydrography to the observed velocity field from surface drifters and subsurface floats.

5.1. Geoid Error Estimates

[39] To evaluate the accuracy of the geoid is a difficult task. In practice, the formal errors for the geoid underestimate the true error in the geoid and smoothing the geoid

with spatial filters complicates the error calculation further. The full error covariance matrix, which for a geoid out to degree and order 200 would be a matrix 40401×40401 , would be nearly impossible to compute and utilize.

[40] Therefore, in order to assess the accuracy of the temporal mean geoid, two empirical methods were used. Both of these error estimates only evaluate the errors of commission in the geoid undulation. The first uses the set of approximately monthly geoids from UT-CSR solutions, which were synthesized into geoid undulation and smoothed as the previous fields were. These 20 geoids are complete to degree and order 120 and are estimated using subsets of the full GRACE data set. Using this set of 20 fields, an area-averaged RMS of them was computed for various smoothing scales and is shown in Table 2. These geoids will likely overestimate the error in the temporal mean geoid because the monthly geoids are computed with less data, only 24–28 days of data, whereas the mean geoid was computed with 363 days of data. Additionally, there is true time variability in the geoid [Wahr *et al.*, 1998]. This temporal geoid variability is small, but does add variance to the estimation of the mean.

[41] The second method for assessing the error is to compare the estimated geoid from the set of mean fields from UT-CSR, NASA-JPL and GFZ, which gives an ensemble of four estimates of the geoid. The four different time-averaged geoids are derived from GRACE, two of which are produced by CSR (one which is combined with terrestrial gravity, and another which does not), one from

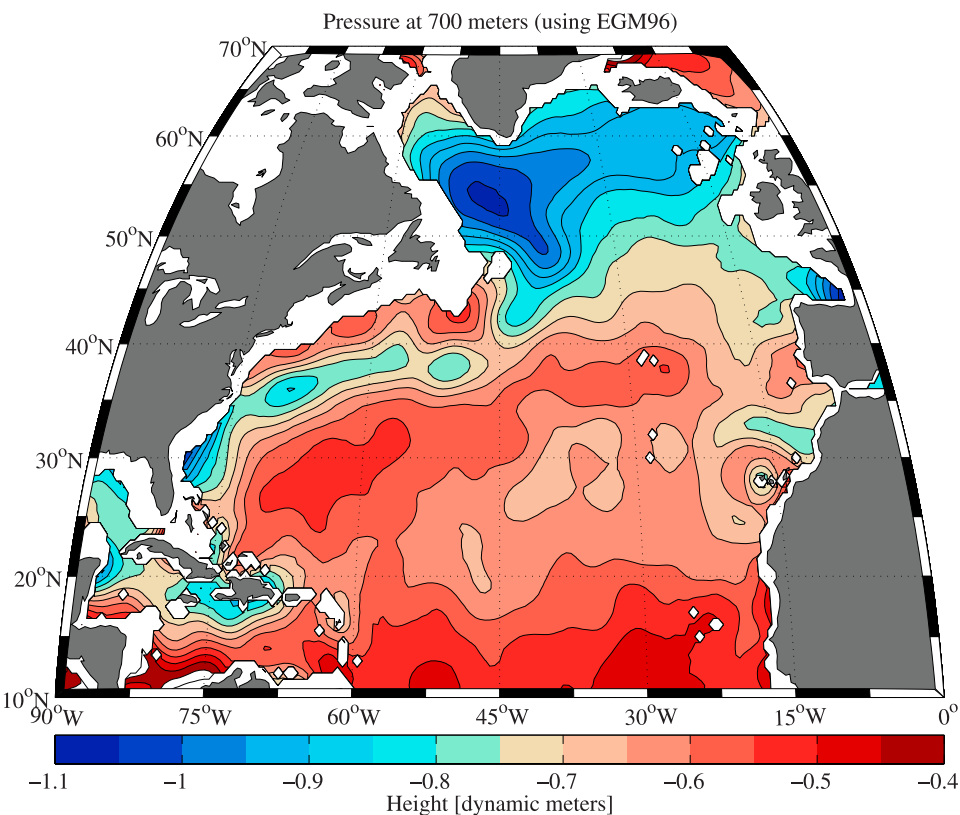


Figure 7. Pressure at 700 m, showing difference of smoothed fields from the CLS01 sea surface height and EGM96 geoid combined with dynamic height from 0 to 700 m. Pressure is in units of equivalent sea surface height. To retrieve pressure, multiply by gravity and density ($9.8 \text{ m s}^{-2} \times 1025 \text{ kg m}^{-3}$).

JPL, and one from GFZ [Reigber *et al.*, 2005]. These were used as a second ensemble and the area-averaged RMS between the fields is shown in Table 2. These were used to synthesize the geoid undulation and smoothed, and the area-averaged RMS between the fields was then computed. The geoids from the different centers use different subsets of the GRACE data set, but should largely represent the same mean, and so this is likely a better estimate of the error in the geoids.

[42] It is noted that the error between the mean geoid estimates from the three centers is less than the RMS differences in the monthly fields. This could arise from true natural variability in the gravity field, or from higher noise in the monthly solutions arising from the use of less data in the monthly fields. In either case, these error estimates represent the lower and upper bounds on the geoid error. For $N = 60$ (resolution = 333 km), which is the case used for most of the presentation here, the committed error in geoid appears to be about 1 cm.

[43] A comparison was also made between the GRACE geoid and the EGM96 geoid. This was estimated by comparing the area-averaged RMS difference of the UT-CSR geoid to the EGM96 geoid. It is found that over the range of low degrees, the differences between the geoids was approximately 5 cm, increasing to an accumulated error of 10 cm at degree and order 100, at which point the differences between the EGM96 geoid and different GRACE geoids are of the same size.

5.2. Sea Surface Height Error Estimates

[44] The error in the sea surface height can be estimated more directly, since the CLS01 mean sea surface height provides an estimated error for their solution at each point. We computed the weighted sum of the squared error for the smoothed sea surface height field, essentially assuming that the error between each point is uncorrelated or that the error covariance matrix is diagonal. However, there is reason to believe that this results in an error map that is optimistic since it neglects systematic biases and correlated measurement errors, such as geographically correlated

Table 2. Error Estimates for Different Smoothing Scales Computed From an Ensemble of Monthly Geoid Estimates, an Ensemble of Four Different Mean GRACE Geoids, and the Difference Between the GRACE Geoid (GGM02C) and EGM96^a

N (Degree and Order)	Resolution, km	Monthly RMS, cm	Means RMS, cm	EGM96 RMS, cm
30	667	0.21	0.27	5.53
40	500	0.27	0.38	6.86
50	400	0.53	0.43	7.85
60	333	1.26	0.79	8.60
70	286	2.81	1.73	9.18
80	250	4.78	3.72	9.64
90	222	6.81	6.96	10.01
100	200	8.71	10.95	10.32

^aError is given in centimeters.

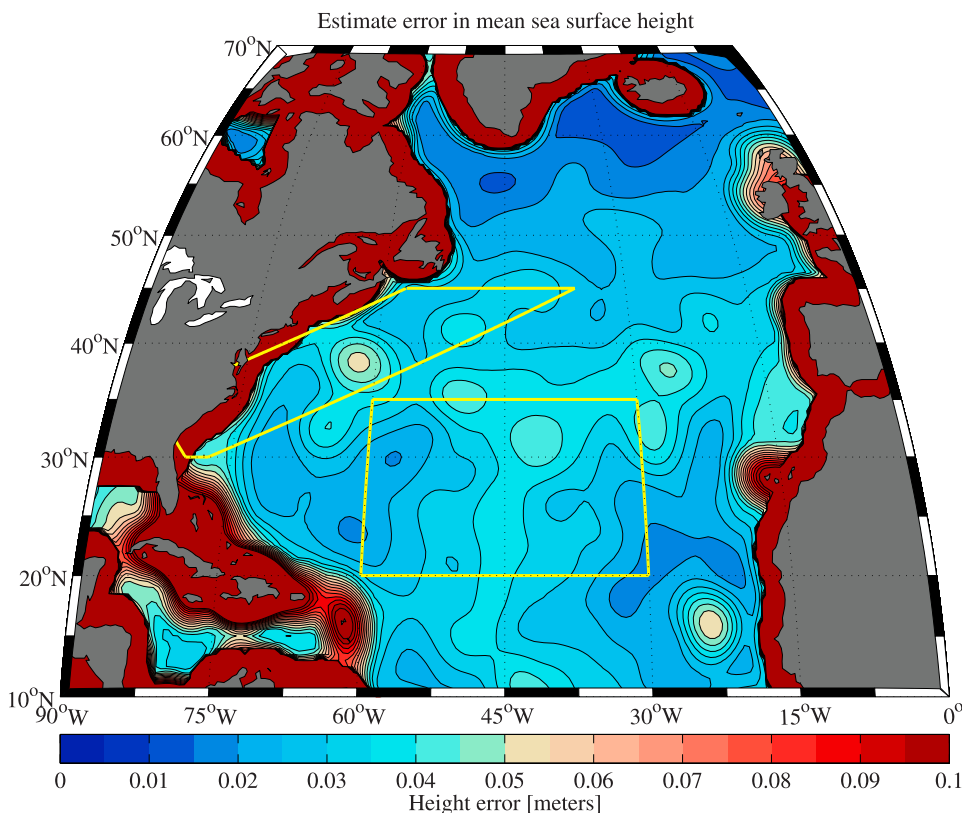


Figure 8. Error in the estimated mean sea surface height computed from the CLS01 sea surface height.

orbit error, aliased tidal errors, and sea state bias errors. However, lacking any information on the true error covariance matrix for the mean sea surface, we take the smoothed error map as a rough measure of true error, and expect that it would need to be scaled in amplitude to reflect the true error in the smoothed mean sea surface height.

[45] The estimated error for the smoothed field is shown in Figure 8. Note the large areas of error in the coastal regions that arise from the extrapolation of the sea surface height toward the coasts, and the general lack of altimetric data near the coasts, because of the loss of tracking by the radar altimeters near the coast. The relatively high error in the Gulf Stream region results from the meandering of the stream and eddy activity leading to a higher variance in the observed sea surface height there. There is also a large area of high error around Cuba, Hispanolia and the other Caribbean islands, which may explain the anomalous low sea surface height in that area.

5.3. Velocity Field Error Estimates

[46] Another method of assessing the error in the derived pressure fields is to compute the geostrophic velocity from the pressure fields and compare them to the observed velocity fields from the floats and drifters. Since the observed velocity fields contain the entire spectrum of wave numbers (down to the spatial binning size) this method of finding the smoothing scale with the minimum error includes both the errors of omission and the errors of commission. We computed the geostrophic velocities at

the bin-averaged drifter and float locations from the derived surface pressure and deep pressure field, and compared them to drifter and float observations respectively. As a measure of the error, we show first the magnitude of the velocity error as

$$\text{error} = |\vec{U}_{obs} - \vec{U}_{geo}|, \quad (6)$$

where \vec{U}_{obs} is the observed drifter or float velocities, and \vec{U}_{geo} is the geostrophic velocity computed from the pressure field. The error maps are shown in Figures 9a, 10a and 11a for the surface, 700 and 2000 m, respectively. The errors in the surface velocity field are dominated by the errors in the high-current areas, namely, the Gulf Stream, the North Atlantic Current, and the Labrador Sea. The error over most of the interior is quite small, less than 5 cm s^{-1} . The errors at 700 m follow a similar picture, though are smaller in magnitude. At 2000 m, the paucity of data makes it difficult to see any pattern, but again it is generally consistent with there being higher errors in the strong current regimes, and lower errors elsewhere.

[47] As a measure of the error this can be slightly misleading since the estimated velocities from the pressure gradients in strong current regime are going to be weaker because of the smoothing applied to the pressure field. Hence in areas where the currents are large, the absolute error will be large as well, and indeed, the error

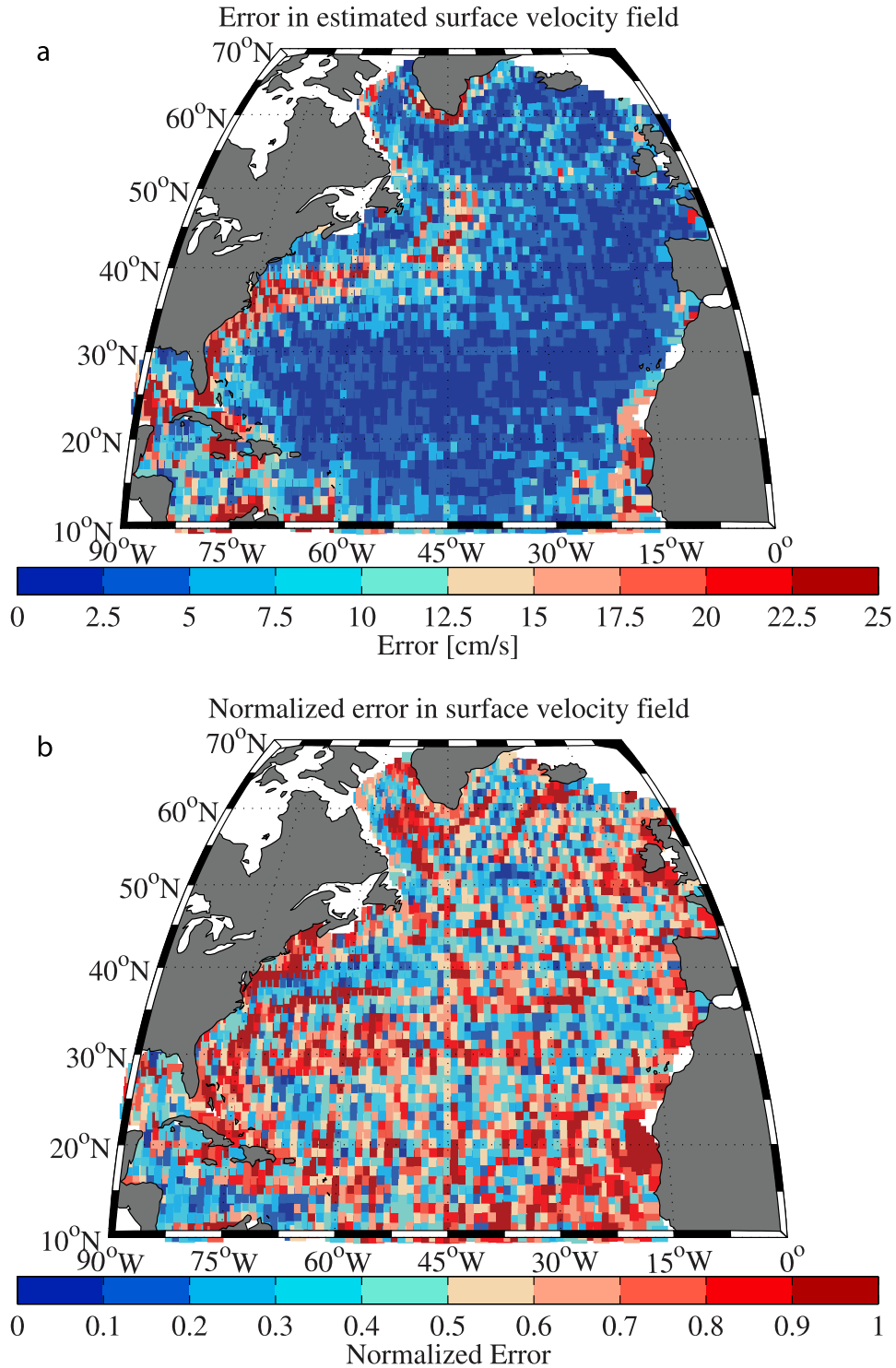


Figure 9. (a) Absolute and (b) normalized error for estimated surface circulation from dynamic ocean topography compared to drifter observations.

map looks similar to a map of velocity magnitude. As a second measure of the error we compute a normalized error as

$$\text{normalized error} = 0 \leq \frac{|\vec{U}_{obs} - \vec{U}_{geo}|}{|\vec{U}_{obs}| + |\vec{U}_{geo}|} \leq 1. \quad (7)$$

A normalized error of 0 would indicate perfect estimation of the current, whereas a value of 1 would indicate the estimated velocity is of the right magnitude but in the opposite direction. Figures 9b, 10b and 11b show that the normalized error in the strong current regions is relatively small, whereas the normalized errors in the interior, where the velocities are small, have larger relative errors. It is

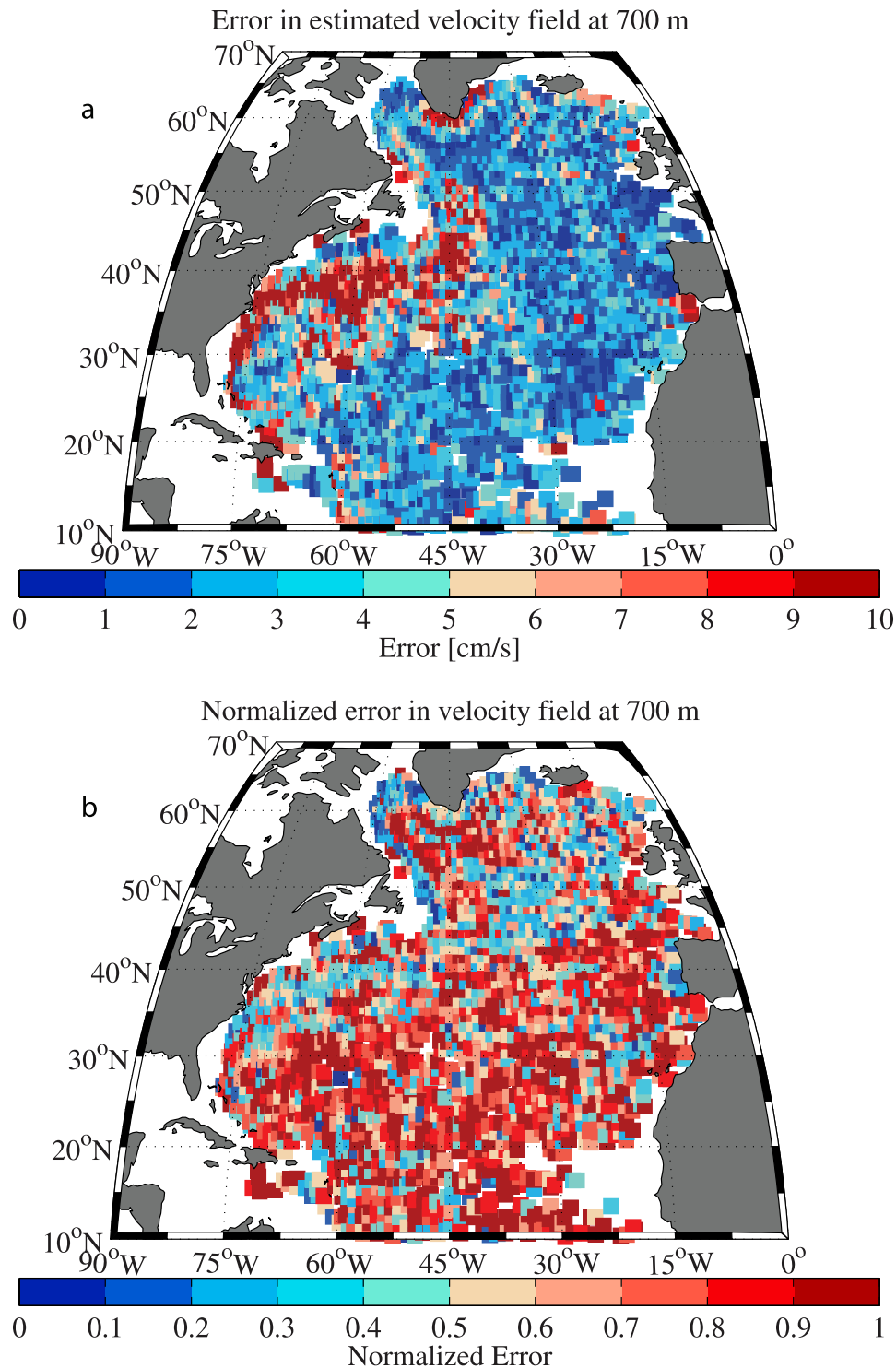


Figure 10. (a) Absolute and (b) normalized error for estimated circulation at 700 m from estimated pressure at 700 m compared to float observations.

difficult to attribute this error to either source since the velocity field in the interior has a relatively small signal-to-noise ratio because of the presence of mesoscale eddies.

[48] We compute spatial averages of the velocity error, over the entire North Atlantic, and the subregions of the Gulf Stream and the interior of the basin, for the surface velocity, and over the entire basin for the velocities at

700 and 2000 m (Table 3). On the whole the pressure fields appear to most consistent with the velocity observations from floats and drifters at a smoothing scale around $N = 60$. For the surface drifters, averaged over the whole North Atlantic, the lowest error occurs at $N = 70$. However, in the region of the Gulf Stream, the errors are continually reduced with increasing wave number,

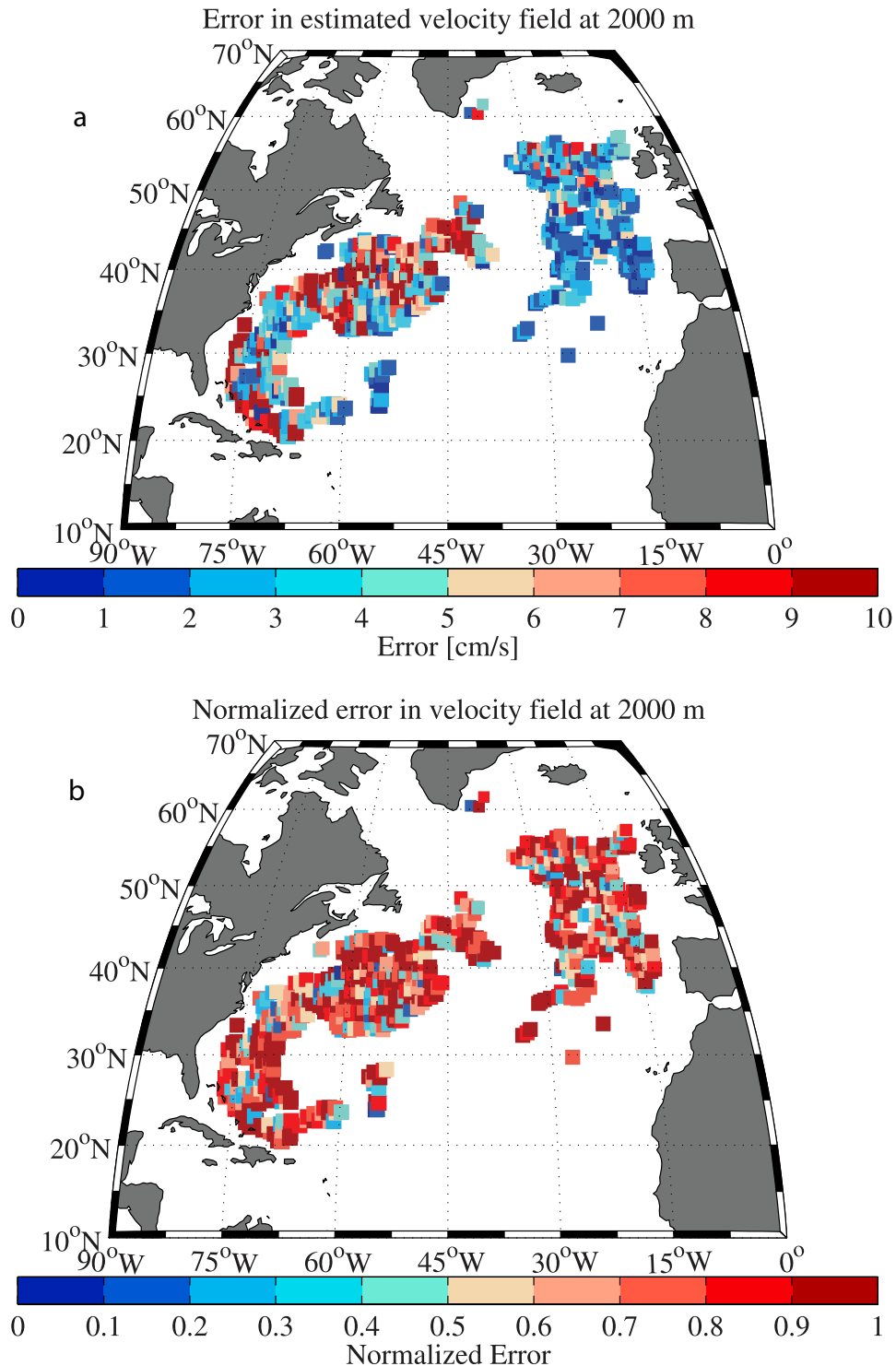


Figure 11. (a) Absolute and (b) normalized error for estimated circulation at 2000 m from estimated pressure at 2000 m compared to float observations.

consistent with our previous analysis (Figure 3) that the time-averaged Gulf Stream is considerably narrower than the smoothed estimates from the dynamic ocean topography can currently give. In the quiescent interior part of the ocean basin, the lowest error is reached at around $N = 50-60$. At higher wave numbers, the geoid error begins to appear as meridional strips. These occur because the

high-degree, low-order harmonics of the geoid are not as well determined by GRACE, though this problem should improve with longer spans of GRACE data are acquired [Tapley *et al.*, 2003b]. Again, there is a trade-off to be made in determining the best smoothing scale. In the Gulf Stream region, the errors of omission are reduced by including the higher wave numbers, and hence reducing

the smoothing scale. In the interior, however, the errors of commission from the higher wave numbers begin to weigh more heavily than the omitted part of the spectrum earlier. At 700 m, the minimum error occurs at around $N = 50-60$. Finally, at 2000 m, the signal-to-noise ratio in the float observations is very small, and there is no reduction in the error variance using the pressure estimated at 2000 m from the mean dynamic topography and the hydrography.

6. Discussion

[49] The GRACE geoid represents a substantial improvement over previous best estimates of the geoid [i.e., Lemoine *et al.*, 1998] for the purposes of estimating the time-averaged ocean circulation when used in combination with satellite altimetric observations of the sea surface height. The GRACE geoid allows the calculation of the temporally averaged dynamic ocean topography, from which the ocean's near surface geostrophic circulation can be calculated. While the temporal mean ocean circulation is an artefact of time averaging, and does not represent the circulation at any point in time, it is necessary for calculating the full near-surface geostrophic circulation from altimeters. As such it is necessary to evaluate its precision with independent data sources.

[50] It appears that the current GRACE geoid is useful for estimating the temporal mean circulation at a resolution of about 300 km. This limit was found by comparing the estimated geostrophic circulation from the dynamic ocean topography with an independent data set of surface drifters and subsurface floats. It is anticipated that the future estimates of the geoid will continue to improve with additional data accumulated during the GRACE mission.

[51] Looking forward, the GOCE (Gravity Field and Steady State Ocean Circulation Explorer) mission should permit the estimation of the mean dynamic ocean topography at the level of 1 cm accuracy on length scales of 100 km [Rio *et al.*, 2004]. At these length scales, the paucity of hydrographic data in some areas of the ocean will become problematic. The Argo float program [Roemmich and Owens, 2000] will help this problem by providing additional hydrographic profiles along with additional float velocity observations at the 2000 m depth. Eventually, one can envision within the next decade being able to make estimates of the time-varying ocean circulation at a 100 km resolution from a combination of altimetry, the geoid, and float velocities and hydrographic profiles. The coastal ocean is poorly observed by the current generation of radar altimeters since they cannot measure the sea surface close to shore. This hinders the estimation of the circulation there. Future altimetry missions such as the proposed Altimetric Bathymetry from Surface Slopes (ABYSS) should be able to recover the near-coastal sea surface height, and improve the estimated dynamic topography in the coast regions.

[52] Ultimately, the best utilization of these data will be through the statistical combination of all the data sets using inverse methods. Efforts toward this goal are currently underway through the Global Ocean Data Assimilation Effort (GODAE), through the assimilation of these observations into dynamical models, i.e., ECCO [Stammer *et al.*, 2003]. Further, the time-varying aspects of the GRACE

Table 3. Velocity Error Estimates for Different Smoothing Scales Averaged Over Different Areas of the North Atlantic for the Surface Circulation Compared to Surface Drifters and the Circulations at 700 and 2000 m Compared to Floats^a

	Resolution, km	North Atlantic Surface	Gulf Stream Surface	Interior Surface	North Atlantic, 700 m	North Atlantic, 2000 m
signal N, deg	—	6.06	16.96	3.17	4.13	4.48
30	667	5.52	15.61	2.69	3.99	4.61
40	500	5.26	14.78	2.62	3.91	4.69
50	400	5.04	13.94	2.57	3.85	4.82
60	333	4.87	13.06	2.58	3.86	5.04
70	286	4.80	12.29	2.71	3.98	5.35
80	250	4.87	11.67	2.99	4.22	5.79
90	222	5.06	11.26	3.36	4.60	6.30
100	200	5.32	11.02	3.75	5.00	6.82

^aSignal refers to the area-averaged drifter and float velocity magnitudes. Signal and error are in cm s^{-1} .

geoids are only beginning to be explored, and should allow the estimation of the time-varying circulation of the deep ocean [Wahr *et al.*, 1998, 2002] and its heat content [Jayne *et al.*, 2003].

[53] **Acknowledgments.** This work was supported by grants NNG04GE95G from the National Aeronautics and Space Administration and OCE 01-37122 from the National Science Foundation and the Young Investigator Program award N00014-03-1-0545 from the Office of Naval Research. Helpful suggestions were made by Terry Joyce, Breck Owens, Carl Wunsch, Victor Zlotnicki, and two anonymous reviewers.

References

- Andersen, O. B., P. Knudsen, and A. L. Vest (2004), The KMS03 multi-mission altimetric mean sea surface, paper presented at ENVISAT Symposium, Eur. Space Agency, Salzburg, Austria, 6–10 Sept.
- Chelton, D. B. (1988), WOCE/NASA Altimeter Algorithm Workshop, *U.S. WOCE Tech. Rep. 2*, U.S. Plann. Off. for WOCE, College Station, Tex.
- Davis, E. S., C. E. Dunn, R. H. Stanton, and J. B. Thomas (1999), The GRACE mission: Meeting the technical challenges, paper IAF-99-B.2.05 presented at Proceedings of 50th International Astronautical Congress, Int. Acad. of Astronaut., Amsterdam, 4–8 Oct.
- Dunn, C., et al. (2003), Instrument of GRACE: GPS augments gravity measurements, *GPS World*, 14, 16–28.
- Ganachaud, A., C. Wunsch, M.-C. Kim, and B. Tapley (1997), Combination of TOPEX/Poseidon data with a hydrographic inversion for determination of the oceanic general circulation and its relation to geoid accuracy, *Geophys. J. Int.*, 128, 708–722.
- Gruber, T., A. Bode, C. Reigber, P. Schwintzer, G. Balmino, R. Biancale, and J.-M. Lemoine (2000), GRIM5-C1: Combination solution of the global gravity field to degree and order 120, *Geophys. Res. Lett.*, 27, 4005–4008.
- Hernandez, F., and P. Schaeffer (2000), Altimetric mean sea surfaces and gravity anomaly maps intercomparisons, *Tech. Rep. AVI-NT-011-5242-CLS*, 44 pp., Coll. Localisation Satell., Ramonville St Agne, France.
- Jayne, S. R., J. M. Wahr, and F. O. Bryan (2003), Observing ocean heat content using satellite gravity and altimetry, *J. Geophys. Res.*, 108(C2), 3031, doi:10.1029/2002JC001619.
- Jekeli, C. (1980), Alternative methods to smooth the Earth's gravity field, *Tech. Rep. Rep. 327*, Dep. of Geod. Sci. and Surv., Ohio State Univ., Columbus.
- Kelly, K. A., T. M. Joyce, D. M. Schubert, and M. J. Caruso (1991), The mean sea surface height and geoid along the Geosat subtrack from Bermuda to Cape Cod, *J. Geophys. Res.*, 96, 12,699–12,709.
- Lavender, K. L., W. B. Owens, and R. E. Davis (2005), The mid-depth circulation of the subpolar North Atlantic Ocean as measured by subsurface floats, *Deep Sea Res., Part I*, 52, 767–785.
- Lemoine, F. G., et al. (1998), The development of the joint NASA GSFC and NIMA geopotential model EGM96, *NASA Tech. Rep. NASA/TP-1998-20681*, Goddard Space Flight Cent., Greenbelt, Md.
- Lozier, S. M., W. B. Owens, and R. G. Curry (1995), The climatology of the North Atlantic, *Prog. Oceanogr.*, 36, 1–44.
- Mann, C. R. (1967), The termination of the Gulf Stream and the beginning of the North Atlantic Current, *Deep Sea Res. Oceanogr. Abstract*, 14, 337–359.

- McCarthy, D. D. (1996), IERS conventions, *Tech. Rep. 21*, Int. Earth Rotation Serv., Paris.
- Niiler, P. P., N. A. Maximenko, and J. C. McWilliams (2003), Dynamically balanced absolute sea level of the global ocean derived from near-surface velocity observations, *Geophys. Res. Lett.*, *30*(22), 2164, doi:10.1029/2003GL018628.
- Olbers, D., J. M. Wenzel, and J. Willebrand (1985), The inference of North Atlantic circulation patterns from climatological hydrographic data, *Rev. Geophys.*, *23*, 313–356.
- Pazan, S. E., and P. P. Niiler (2004), New global drifter data set available, *Eos Trans. AGU*, *85*, 17.
- Priestley, M. B. (1981), *Spectral Analysis and Time Series*, vol. 1, *Univariate Series*, vol. 2, *Multivariate Series, Prediction and Control*, Elsevier, New York.
- Ralph, E. A., and P. P. Niiler (1999), Wind-driven currents in the Tropical Pacific, *J. Phys. Oceanogr.*, *29*, 2121–2129.
- Rapp, R. H., Y. M. Ming, and N. K. Pavlis (1991), The Ohio State 1991 geopotential and sea surface topography harmonic coefficient model, *Tech. Rep. 410*, Dep. of Geod. Sci. and Surv., Ohio State Univ., Columbus.
- Reid, J. L. (1994), On the total geostrophic circulation of the North Atlantic Ocean: Flow patterns, tracers, and transports, *Prog. Oceanogr.*, *33*, 1–92.
- Reigber, C., R. Schmidt, F. Flechtner, R. König, U. Meyer, K.-H. Neumayer, P. Schwintzer, and S. Y. Zhu (2005), An Earth gravity field model complete to degree and order 150 from GRACE: EIGEN-GRACE02S, *J. Geodyn.*, *39*, 1–10.
- Rio, M.-H., F. Hernandez, and J.-M. Lemoine (2004), Estimate of a global mean dynamic topography combining altimetry, in situ data and a geoid model: Impact of GRACE and GOCE data, paper presented at Second International GOCE User Workshop "GOCE, the Geoid and Oceanography", Eur. Space Agency, Frascati, Italy, 8–10 March.
- Roemmich, D., and W. B. Owens (2000), The Argo project: Global ocean observations for understanding and prediction of climate variability, *Oceanography*, *13*, 45–50.
- Schröter, J., M. Losch, and B. Sloyan (2002), Impact of the Gravity Field and Steady-State Ocean Circulation Explorer (GOCE) mission on ocean circulation estimates: 2. Volume and heat fluxes across hydrographic section of unequally spaced stations, *J. Geophys. Res.*, *107*(C2), 3012, doi:10.1029/2000JC000647.
- Smith, D. A. (1998), There is no such thing as "The" EGM96 geoid: Subtle points on the use of a global geopotential model, *Int. Geoid Serv. Bull.*, *8*, 17–28.
- Stammer, D., and C. Wunsch (1994), Preliminary assessment of the accuracy and precision of TOPEX/Poseidon altimeter data with respect to the large-scale ocean circulation, *J. Geophys. Res.*, *99*, 24,584–24,604.
- Stammer, D., C. Wunsch, R. Giering, C. Eckert, P. Heimbach, J. Marotzke, A. Adcroft, C. N. Hill, and J. Marshall (2003), Volume, heat and freshwater transports of the global ocean circulation 1993–2000, estimated from a general circulation model constrained by World Ocean Circulation Experiment (WOCE) data, *J. Geophys. Res.*, *108*(C1), 3007, doi:10.1029/2001JC001115.
- Stephens, J. I., T. P. Antonov, T. P. Boyer, M. E. Conkright, R. A. Locarnini, T. D. O'Brien, and H. C. Garcia (2002), *World Ocean Data Atlas, 2001*, vol. 1, *Temperature*, NOAA Atlas, NESDIS 49, NOAA, Silver Spring, Md.
- Tapley, B. D., and M.-C. Kim (2001), Applications to geodesy, in *Satellite Altimetry and Earth Sciences*, *Int. Geophys. Ser.*, vol. 69, edited by L.-L. Fu and A. Cazenave, chap. 10, pp. 371–406, Elsevier, New York.
- Tapley, B. D., S. Bettadpur, M. Cheng, D. Hudson, and G. Kruizinga (2003a), Early results from the Gravity Recovery and Climate Experiment, paper AAS 03–622 presented at AAS/AISS Astrodynamic Specialists Conference, Am. Astronaut. Soc., Big Sky, Mont., 3–7 Aug.
- Tapley, B. D., D. P. Chambers, S. Bettadpur, and J. C. Ries (2003b), Large scale ocean circulation from the GRACE GGM01 Geoid, *Geophys. Res. Lett.*, *30*(22), 2163, doi:10.1029/2003GL018622.
- Tapley, B. D., S. Bettadpur, M. Watkins, and C. Reigber (2004), The Gravity Recovery And Climate Experiment: Mission overview and early results, *Geophys. Res. Lett.*, *31*, L09607, doi:10.1029/2004GL019920.
- Tapley, B. D., et al. (1996), The Joint Gravity Model 3, *J. Geophys. Res.*, *101*, 28,029–28,049.
- Tapley, B. D., et al. (2005), GGM02—An improved Earth gravity field model from GRACE, *J. Geod.*, *79*, 467–478, doi:10.1007/s00190-005-0480-z.
- Wahr, J., M. Molenaar, and F. Bryan (1998), Time variability of the Earth's gravity field: Hydrological and oceanic effect and their possible detection using GRACE, *J. Geophys. Res.*, *103*, 30,205–30,229.
- Wahr, J. M., S. R. Jayne, and F. O. Bryan (2002), A method of inferring changes in deep ocean currents from satellite measurements of time variable gravity, *J. Geophys. Res.*, *107*(C12), 3218, doi:10.1029/2001JC001274.
- Wang, Y. M. (2000), The satellite altimeter data derived mean sea surface GSF098, *Geophys. Res. Lett.*, *27*, 701–704.
- Wunsch, C., and E. M. Gaposchkin (1980), On using satellite altimetry to determine the general circulation of the oceans with application to geoid improvement, *Rev. Geophys.*, *18*, 725–745.
- Wunsch, C., and D. Stammer (1998), Satellite altimetry, the marine geoid, and the oceanic general circulation, *Annu. Rev. Earth Planet. Sci.*, *26*, 219–253.
- Wunsch, C., and D. Stammer (2003), Global ocean data assimilation and geoid measurements, *Space Sci. Rev.*, *108*, 147–162.
- Zlotnicki, V. (1984), On the accuracy of gravimetric geoids and the recovery of oceanographic signals from altimetry, *Mar. Geod.*, *8*, 129–157.

S. R. Jayne, Department of Physical Oceanography, Woods Hole Oceanographic Institution, MS 21, 360 Woods Hole Road, Woods Hole, MA 02543-1541, USA. (surje@alum.mit.edu)